RSC Advances

PAPER

View Article Online
View Journal | View Issue

Cite this: *RSC Adv.*, 2019, **9**, 17335

Novel polythiophene derivative for dual-channel cell imaging

Fengyan Wang, *[ab] Huiyun Xia,[a] Siyu Pu,[a] Ni Yan,[a] Jiale Song,[a] Yefei Tian,[a] Junji Wei[a] and Luke Yan[ab]

Received 19th February 2019
Accepted 23rd May 2019

DOI: 10.1039/c9ra01262a

rsc.li/rsc-advances

Fluorescent materials play an extremely important role in understanding the microbiological world. New fluorescent materials which have good photophysical properties, low cytotoxicity, and multi-channel fluorescent imaging capability are still urgently needed, even though many kinds of fluorescent materials have already been synthesized. In this work, a new polythiophene derivative (PT-OH-PPR) modified with a porphyrin group in its side chain was designed and fabricated through $FeCl_3$ oxidative polymerization. The obtained PT-OH-PPR has wide absorption and emission spectral range, good water solubility and low cytotoxicity. Importantly it could be enriched in the cytoplasm of A549 cells and be excited by two excitation wavelengths (488 nm and 559 nm), which provides a promising application in dual-channel cell imaging.

1 Introduction

With the development of biotechnology and the increasing use of biological products, various biological assay methods and techniques have been developed. Among them, fluorescent materials play an extremely important role due to their wide application in flow cytometry, fluorescence microscopy and so on.[1–3] Quantum dots,[4–6] organic dyes,[7–9] and engineered fluorescent proteins[10–12] are commonly used fluorescent materials. Yet their further applications have been limited as a result of fast photobleaching defects of organic dyes and engineered fluorescent proteins,[13–16] and surface modification difficulties and heavy-metal core-related cytotoxicity of quantum dots.[17,18] Hence, there is a pressing need to design and synthesize new fluorescent materials possessing good photostability and low cytotoxicity.

Conjugated polymer (CP) is a kind of fluorescent material composed of many conjugated light absorbing units. The delocalized electronic structure endows its strong light-trapping ability and unique fluorescence signal amplification effects, which gives it a significant advantage in the bioimaging field.[19–22] Introducing ionic groups (sulfhydryl group, carboxyl group, quaternary ammonium group, *etc.*) into the side chains of conjugated polymers could obtain water-soluble conjugated polymers (WSCPs).[23–26] WSCPs have several advantages for *in vitro*/*vivo* bioimaging applications, such as high fluorescence brightness, good photostability, and easy modulation of the absorption and emission spectra.[27–29] Targeted recognition and imaging of cells could be achieved by attaching various specific recognition groups to the side chains of WSCPs.[30–32] For example, in 2017, Jiang and coworkers covalently attached galactose to the side chain of poly(*p*-phenyleneethynylene), and achieved targeted imaging of hepatoma cell.[33] Moreover, Lu and coworkers synthesized $PTCO_2$ (poly[3-(3-*N*,*N*-diacetateaminopropoxy)-4-methyl thiophene disodium salts]) that could form $PTCO_2$–Cu(II) ensemble with Cu^{2+}. In addition, they successfully used Cys to regulate the imaging ability of $PTCO_2$–Cu(II) in HeLa cells.[34] However, there are few studies on multi-channel cell imaging using a single water-soluble conjugated polymer probe.

Herein, a new polythiophene derivative (PT-OH-PPR) modified with a porphyrin group in its side chain was designed and fabricated through $FeCl_3$ oxidative polymerization. Porphyrin derivatives have characteristic UV-vis absorption and emission spectra including single absorption peak around 420 nm (Soret band), four weak absorption peaks between 500 nm and 700 nm (Q band), and two emission peaks between 620 nm and 750 nm. Thus, the introduced porphyrin group could broaden both the absorption and emission range of PT-OH-PPR. Also, PT-OH-PPR has good water solubility and low cytotoxicity. Furthermore, it could enrich in the cytoplasm of A549 cells and be excited by two excitation wavelengths (488 nm and 559 nm), which provides a promising application in dual-channel cell imaging.

2 Experimental section

2.1 Materials and instruments

All organic solvents and anhydrous ferric chloride were bought from Sinopharm Chemical Reagent Beijing Co., Ltd. Monomer

[a]School of Materials Science & Engineering, Chang'an University, Xi'an 710064, China. E-mail: wfy0914@chd.edu.cn
[b]Engineering Research Center of Transportation Materials, Ministry of Education, Chang'an University, Xi'an 710064, China

1, 2 and PPR were prepared referring to reported synthetic methods.[35,36] MTT (methylthiazolyldiphenyl-tetrazolium bromide) and FBS (fetal bovine serum) were bought from Xinjingke Biotechnology Co., Ltd (Beijing, China). DMEM (Dulbecco's modified Eagle medium) used to culture cells was purchased from HyClone/Thermofisher. Lyso Tracker Red DND-99 and Hoechst 33342 were bought from Invitrogen. PBS (phosphate buffer saline) and Trypsin Solution (0.25%) were obtained from GIBCO. A549 cell lines were purchased from cell culture center of the Institute of Basic Medical Sciences, Chinese Academy of Medical Sciences (Beijing, China). Double distilled water treated with a Millipore filtration system was used in the experiment. Cell culture related consumables were purchased from Nunc. Fluorescence quantum yields were determined based on fluorescein (0.79). The ^{1}H NMR spectra were conducted with a Bruker Avance 400 MHz spectrometer. UV-vis absorption spectra were measured with a JASCOV-550 spectrophotometer. Fluorescence spectra and photostability testing after irradiating with white light (CEL-HXF300/CEL-HXUV300, AuLight) were recorded on a Hitachi F-4500 fluorimeter. Dynamic light scattering (DLS) experiments were supplied by a Zetasizer Nano ZS90 (Malvern) system. *In vitro* cell viability assay was measured with a microplate reader (BIO-TEK Synergy HT, USA). Confocal laser scanning microscopy (CLSM) characterization was recorded on a confocal laser scanning biological microscope (FV1000-IX81, Olympus, Japan).

2.2 Synthesis of PT-OH-PPR

A solution of monomer 1 (39 mg, 0.102 mmol), 2 (7.6 mg, 0.029 mmol) and PPR (13.4 mg, 0.0146 mmol) in $CHCl_3$ (10 mL) was deaerated before addition of anhydrous $FeCl_3$ (107 mg, 0.657 mmol). Subsequently, the reaction mixture was kept away from light and stirred under N_2 atmosphere for 48 h. The liquid was abandoned and the remaining solid was continuously dissolved with CH_3OH until the solid could no longer be dissolved. To the combined methanol phase, hydrazine hydrate was added drop by drop until no further precipitate was formed. After centrifugation, collected and then concentrated the supernatant under vacuum to give an orange-red coarse product. The coarse product was dissolved in DMSO (1 mL) and then diluted with 9 mL water. A dialysis bag (molecular weight cutoff: 3500) was used to load the aforementioned solution. The bag was then put into a water bath for dialyzing. After nine times dialyzing, the resulted solution was freeze-dried to afford 12 mg red sticky substance (yield 20%). ^{1}H NMR (400 MHz, DMSO-d6, δ): 8.56 (br, 8.00H), 8.09 (br, 8.48H), 7.55 (br, 6.16H), 7.23–7.42 (br, 23.78H), 4.39 (br, 2.55H), 4.10 (br, 2.59H), 3.78–4.00 (br, 50.05H), 3.40–3.78 (br, 304.12H), 3.21–3.40 (br, 179.26H), 2.90–3.21 (br, 252.17H), 2.74–2.87 (br, 31.81H), 2.68 (br, 19.88H), −2.93 (br, 2.18H).

2.3 Particle size characterization

The ultrapure aqueous solution of PT-OH-PPR (1 mL, 100 μM) was added into the special particle size measuring cell. The cell was then put into the Zetasizer Nano ZS90 (Malvern) system. The temperature was 25 °C, and the balance time was 2 min. Then, the particle size was measured in parallel for three times.

2.4 Photostability assay of PT-OH-PPR

To a disposable fluorescent colorimetric dish, the aqueous solution of PT-OH-PPR (30 μM, 1 mL) was added. To another disposable fluorescent colorimetric dish, an aqueous solution of Lysotracker Red DND-99 (10 μM, 1 mL) was added. The above samples were irradiated under white light (6 mW cm^{-2}, 12 min), meanwhile, their fluorescence intensity was recorded every two minutes using a Hitachi F-4500 fluorimeter.

2.5 Cell culture and passage

A549 cells were placed in a cell culture dish (60 mm), and DMEM medium containing 10% FBS (3 mL) was added. Then the dish was put in a humidified incubator (condition: 37 °C, 5% CO_2) for cultivation. As A549 cells are adherent cells, when they occupied 80% of the bottom area, the cell culture medium was discarded and 0.25% trypsin solution (1 mL) was added to digest them in a humidified incubator for 3 min. Fresh medium (10% FBS in DMEM, 2 mL) was added in order to stop the digestion of trypsin. A549 cells in the bottom of the dish were repeatedly blew with a liquid shifter so that they could be fully dispersed. The obtained cell suspension was centrifugated (1000 rpm, 5 min), the supernatant was discarded and a certain amount of fresh medium was added. Then, the cells were re-dispersed. One-third of the cells were pipetted into a new culture dish and continued to culture for later use.

2.6 Cell viability assay by MTT

After digestion, centrifugation, and resuspension with fresh medium, the cell density of the obtained A549 cell suspension was counted using a cell counter. The cells were diluted with fresh medium to the density of 1×10^5 cells per milliliter. Then 100 μL of the above solution was added into each hole of a 96-well plate (1×10^4 cells per well). The plate was then put into the humidified incubator for 20 h cultivation. The supernatant in each hole of the aforementioned 96-well plate was abandoned, and then 100 μL fresh medium with various concentrations of PT-OH-PPR was added. The plate was replaced into the humidified incubator and continued culturing for 24 h. The supernatant in each well was abandoned again, 100 μL fresh medium and 10 μL MTT (5 mg mL^{-1}) was added into each well, and continued culturing for 4 h. Then the supernatant in each well was replaced by 100 μL dimethyl sulfoxide in order to dissolve the generated formazan. The plate was put into a microplate reader and shook for 5 min to fully dissolve the formed formazan. Then the absorbance of the purple formazan (490 nm) was recorded. The cell viability rate (VR) was calculated on the basis of the following equation in which A and A_0 stand for the absorbance of the experimental group and control group respectively.

$$\mathrm{VR} = \frac{A}{A_0} \times 100\%$$

2.7 Cell imaging experiment

A549 cells (about 8×10^4 cells) were seeded in a culture plate (Nunc, 35 mm). After 12 h incubation in the humidified incubator, the culture medium was replaced by 1 mL fresh DMEM medium containing 20 μM PT-OH-PPR and continued culturing for 24 h. The supernatant was discarded, and the cells were washed thrice with 1 × PBS followed by fixing with paraformaldehyde (4% in PBS) for 20 min at room temperature. After washing thrice with 1 × PBS, 1 mL 1 × PBS and 10 μL Hoechst 33342 (10 mg mL^{-1}) were added into the plate in turn so as to stain the cell nuclei. After staining for five minutes at room temperature and washing thrice with 1 × PBS, the images were taken on CLSM.

3 Results and discussion

3.1 Materials synthesis and characterization

In the presence of $FeCl_3$, PT-OH-PPR was obtained in 20% yield from monomer 1, 2 and PPR through oxidative copolymerization (Scheme 1). The ^1H NMR spectra of monomer 1, 2, PPR and PT-OH-PPR were measured in DMSO-d6 and displayed in Fig. 1. After carefully comparison, we found that the peak marked with a_1 in Fig. 1A is corresponding to that marked with a_1' in Fig. 1D. The characteristic peaks c_1–c_5 of the porphyrin group of PPR are corresponding to that marked with c_1'–c_5' in Fig. 1D. Monomer 1, 2 and PPR successfully copolymerized with each other to form PT-OH-PPR and the actual ratio of them was determined to be 73%, 21% and 6% in turn, after carefully calculating and analyzing the proportion of characteristic hydrogen in Fig. 1D.

3.2 Photophysical properties

Since the quaternary ammonium monomer (monomer 1) dominates, the obtained polymer PT-OH-PPR has good dispersibility in aqueous solution. Fig. 2A showed that the average particle size of the aggregate formed by PT-OH-PPR in aqueous solution was about 28 nm. The photophysical properties of PT-OH-PPR were measured in aqueous solution and showed in Fig. 2B. The maximum absorption peak of PT-OH-PPR was 424 nm which corresponded to the π–π* transition of the conjugated backbone. The extinction coefficient of PT-OH-PPR was 8.6×10^3 L mol^{-1} cm^{-1}. The maximum emission peak was 575 nm for PT-OH-PPR with the Stokes shift of 151 nm and

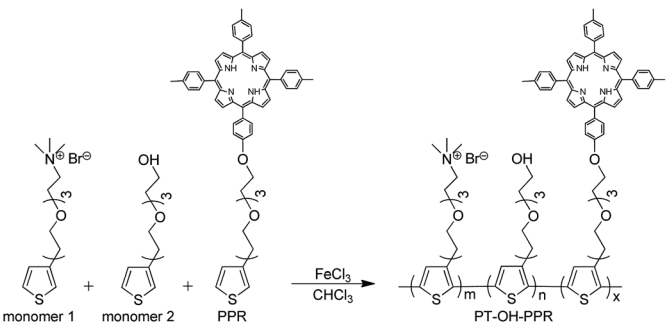

Scheme 1 Synthetic route of PT-OH-PPR.

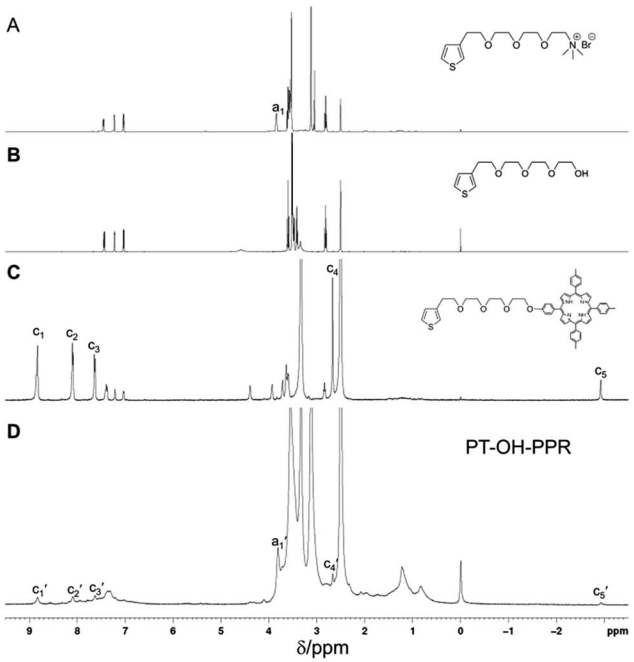

Fig. 1 The ^1H NMR spectra of monomer 1, 2, PPR and PT-OH-PPR in DMSO-d6.

the fluorescence quantum efficiency of 3.1%. A Hitachi F-4500 fluorimeter was used to measure the photostability of PT-OH-PPR. From Fig. 2C we could see that the fluorescence intensity of PT-OH-PPR maintained at more than 51% after 12 min irradiation (6 mW cm^{-2} white light), while the comparison dye Lyso Tracker Red DND-99 maintained at more than 96%. This

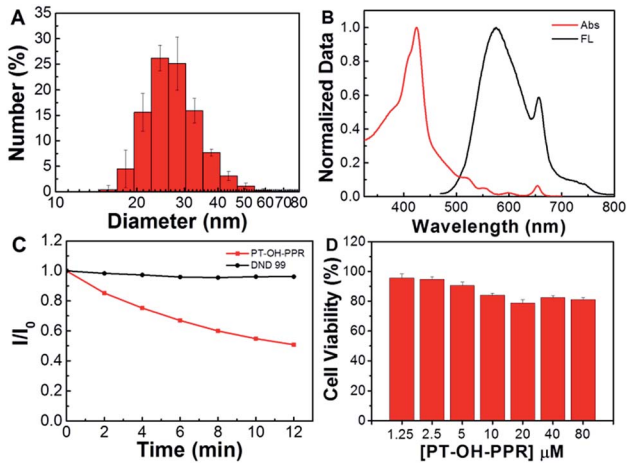

Fig. 2 (A) Hydrodynamic diameter distribution of PT-OH-PPR recorded by DLS. [PT-OH-PPR] = 100 μM in RU. (B) The UV-vis absorption and emission spectra of PT-OH-PPR in aqueous solution after normalization. Excitation wavelength: 460 nm. [PT-OH-PPR] = 100 μM in RU. (C) Photostability of PT-OH-PPR after irradiating with white light (6 mW cm^{-2}, 12 min). [PT-OH-PPR] = 30 μM in RU, [DND-99] = 10 μM. (D) Cell viabilities of A549 cells as a function of different PT-OH-PPR concentrations (1.25, 2.5, 5, 10, 20, 40, 80 μM).

results showed that PT-OH-PPR has a certain photostability, which endows its potential application in the bioimaging field.

3.3 Cell imaging application

As cytotoxicity is a critical factor in bioimaging, the cytotoxicity of PT-OH-PPR against A549 cells was further tested using a typical MTT method. As exhibited in Fig. 2D, after cultured with PT-OH-PPR (1.25, 2.5, 5, 10, 20, 40, 80 μM) for 24 h in a humidified incubator, more than 80% cells were alive, which indicates that PT-OH-PPR does not have any obvious cytotoxicity to A549 cells in dark. Therefore, the low cytotoxicity of PT-OH-PPR ensures its cell imaging and further biological applications.

Then, *in situ* cell imaging experiments of PT-OH-PPR were performed. In the experimental group, A549 cells were incubated with fresh DMEM medium containing PT-OH-PPR (20 μM in RU) for 24 h, then Hoechst 33342 (final concentration: 10 μg mL^{-1}) was used to stain the nucleus. In the control group, cells were incubated with fresh DMEM medium without PT-OH-PPR. As depicted in Fig. 3A, the fluorescence of PT-OH-PPR could not overlap with that of the nuclear dye (Hoechst 33342). Therefore, PT-OH-PPR could enter the cytoplasm of A549 cells, but could not enter the nucleus. Three-dimensional scan images (Fig. 3A-e) further demonstrated that PT-OH-PPR could distribute throughout the whole cytoplasm.

Compared the normalized UV-vis absorption and fluorescent emission spectra of PT-OH-PPR (Fig. 2B) with that of PPR (Fig. 3 in ref. 36), the sharp absorption peak (424 nm) of PT-OH-PPR corresponded to the Soret band of the porphyrin group, the other four weak absorption peaks (515, 552, 596 and 654 nm) corresponded to its Q band. Moreover, the emission peaks (657 and 726 nm) of PT-OH-PPR corresponded to the fluorescence emission of porphyrin. Thus, the absorption and emission scope of PT-OH-PPR was broadened by the introduced

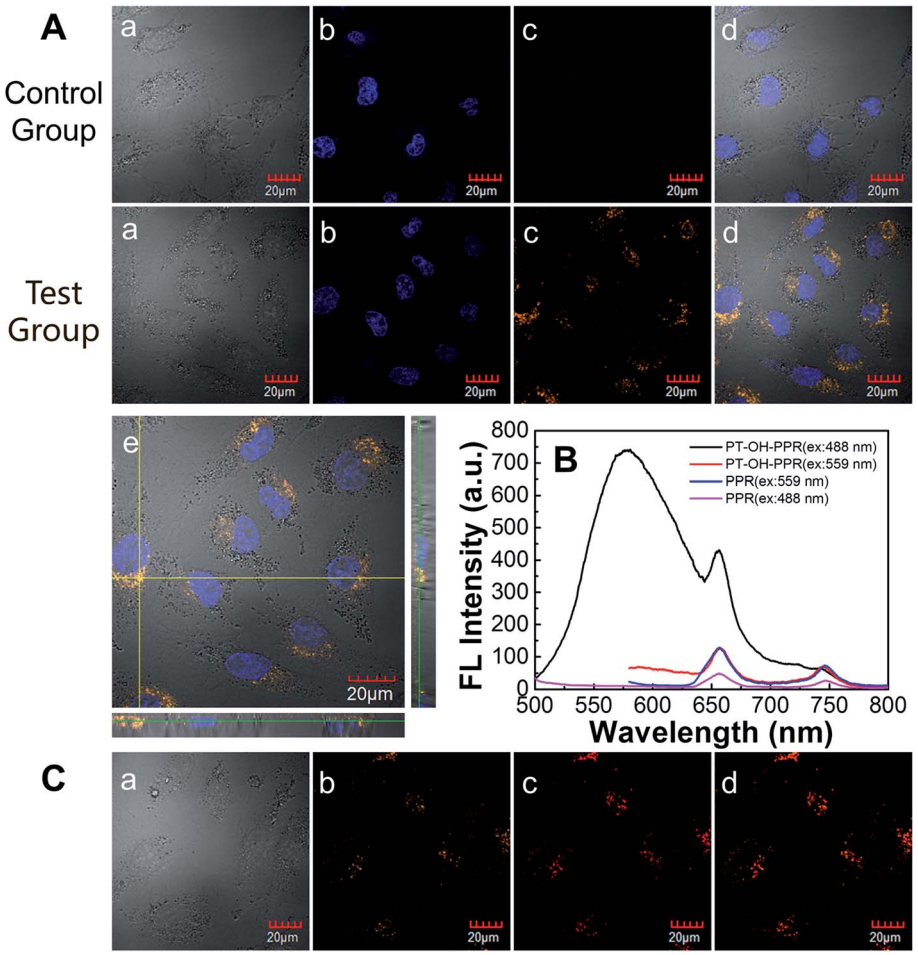

Fig. 3 (A) Location of PT-OH-PPR in A549 cells. Control group: [Hoechst 33342] = 10 μg mL; test group: [PT-OH-PPR] = 20 μM (in RU), [Hoechst 33342] = 10 μg mL^{-1}. (a) Phase contrast image; (b) fluorescence image of Hoechst 33342; (c) fluorescence image of PT-OH-PPR; (d) overlapped image of (b) and (c); (e) three-dimensional scan images. Hoechst 33342 (excitation: 405 nm; collection: 425–475 nm; false color: blue). PT-OH-PPR (excitation: 488 nm; collection: 540–640 nm; false color: orange). (B) Fluorescent emission spectra of PT-OH-PPR and PPR excited by both 488 and 559 nm. [PPR] = 0.6 μM, [PT-OH-PPR] = 10 μM (in RU). (C) Dual-channel fluorescence images of PT-OH-PPR in A549 cells. (a) Phase contrast image; (b) fluorescence image of the conjugated backbone of PT-OH-PPR (excitation: 488 nm; collection: 500–600 nm; false color: orange); (c) fluorescence image of covalently connected porphyrin group (excitation: 559 nm; collection: 655–755 nm; false color: red); (d) overlapped image of (b) and (c). [PT-OH-PPR] = 20 μM (in RU).

porphyrin group. To further verify the aforementioned conclusion, two common excitation wavelengths were chosen to excite PPR (0.6 μM) and PT-OH-PPR (10 μM in RU). As shown in Fig. 3B, under 488 nm excitation the emission intensity of the porphyrin group in PT-OH-PPR was stronger than that of PPR (monomer 3), which certified that an efficient intramolecular fluorescence resonance energy transfer (FRET) occurred from the conjugated backbone to the covalently connected porphyrin group. While the emission intensity of the porphyrin group in PT-OH-PPR is close to that of PPR under 559 nm excitation. This result confirmed that the ratio of PPR monomer calculated by ^{1}H NMR was accurate. Next, *in situ* cell imaging experiment of PT-OH-PPR was performed based on the specific photophysical properties. As depicted in Fig. 3C, PT-OH-PPR entering the cell could be excited by two excitation wavelengths (488 and 559 nm), and the fluorescence images obtained under the two excitation wavelengths could overlap well. Due to the two excitation wavelengths (488 and 559 nm) are widely used in many commercially available bioimaging instruments, PT-OH-PPR is considerable potential in dual-channel cell imaging.

4 Conclusions

In the present work, a new polythiophene derivative (PT-OH-PPR) modified with a porphyrin group in its side chain was designed and fabricated through $FeCl_3$ oxidative polymerization. The spectral characterization results showed that the maximum absorption and emission peaks of PT-OH-PPR were 424 nm and 575 nm, respectively. The molar absorption coefficient was 8.6×10^3 L mol^{-1} cm^{-1}, and the fluorescence quantum efficiency is 3.1%. In addition, the average particle size of the aggregate formed by PT-OH-PPR in aqueous solution was about 28 nm. As PT-OH-PPR had good optical properties and low cytotoxicity, it was used in cell imaging assay. The results indicated that PT-OH-PPR could enter the cytoplasm of A549 cells. Furthermore, PT-OH-PPR could be simultaneously excited by two excitation wavelengths (488 and 559 nm), which endows its potential application in dual-channel cell imaging.

Conflicts of interest

There are no conflicts to declare.

Acknowledgements

The authors would like to thank the Natural Science Foundation of China (Program No. 21704005, 21603016, 51603016, 51703010), National Training Programs of Innovation and Entrepreneurship for Undergraduates (Program No. 201910710489), Student Innovation Practice Ability Enhancement Sub-project of Chang'an University (Program No. 300102319812), Xi'an Science and Technology Planning Project (2017137SF/WM031).

Notes and references

1 B. Wang, J. Song, H. Yuan, C. Nie, F. Lv, L. Liu and S. Wang, *Adv. Mater.*, 2014, **26**, 2371–2375.
2 K. Lee, J. Lee, E. J. Jeong, A. Kronk, K. S. J. Elenitoba-Johnson, M. S. Lim and J. Kim, *Adv. Mater.*, 2012, **24**, 2479–2484.
3 X. Zhang, X. Zhang, B. Yang, S. Wang, M. Liu, Y. Zhang, L. Tao and Y. Wei, *RSC Adv.*, 2013, **3**, 9633–9636.
4 X. Michalet, F. F. Pinaud, L. A. Bentolila, J. M. Tsay, S. Doose, J. J. Li, G. Sundaresan, A. M. Wu, S. S. Gambhir and S. Weiss, *Science*, 2005, **307**, 538–544.
5 Y. Song, S. Zhu and B. Yang, *RSC Adv.*, 2014, **4**, 27184–27200.
6 Y. Wang, R. Hu, G. Lin, I. Roy and K. T. Yong, *ACS Appl. Mater. Interfaces*, 2013, **5**, 2786–2799.
7 S. Fery-Forgues, M. Abyan and J. F. Lamere, *Ann. N. Y. Acad. Sci.*, 2010, **1130**, 272–279.
8 Y. J. Pu, M. Higashidate, K. I. Nakayama and J. Kido, *J. Mater. Chem.*, 2008, **18**, 4183–4188.
9 M. S. Schiedel, C. A. Briehn and P. Bäuerle, *Angew. Chem.*, 2001, **40**, 4677–4680.
10 K. G. Chernov, T. A. Redchuk, E. S. Omelina and V. V. Verkhusha, *Chem. Rev.*, 2017, **117**, 6423–6446.
11 M. W. Davidson and R. E. Campbell, *Nat. Methods*, 2009, **6**, 713–717.
12 D. M. Shcherbakova, M. Baloban and V. V. Verkhusha, *Curr. Opin. Chem. Biol.*, 2015, **27**, 52–63.
13 D. Beer and J. Weber, *Opt. Commun.*, 1972, **5**, 307–309.
14 J. L. Lubbeck, K. M. Dean, R. Jiminez and A. E. Palmer, *Biophys. J.*, 2010, **98**, 584a.
15 J. L. Lubbeck, K. M. Dean, H. Ma, A. E. Palmer and R. Jimenez, *Anal. Chem.*, 2012, **84**, 3929–3937.
16 M. L. Spaeth and W. R. Sooy, *J. Chem. Phys.*, 1968, **48**, 2315–2323.
17 C. E. Bradburne, J. B. Delehanty, G. K. Boeneman, B. C. Mei, H. Mattoussi, K. Susumu, J. B. Blanco-Canosa, P. E. Dawson and I. L. Medintz, *Bioconjugate Chem.*, 2013, **24**, 1570–1583.
18 H. Ron, *Environ. Health Perspect.*, 2006, **114**, 165–172.
19 C. Zhu, Q. Yang, L. Liu and S. Wang, *Chem. Commun.*, 2011, **47**, 5524–5526.
20 C. C. You, O. R. Miranda, B. Gider, P. S. Ghosh, I. B. Kim, B. Erdogan, S. A. Krovi, U. H. F. Bunz and V. M. Rotello, *Nat. Nanotechnol.*, 2007, **2**, 318–323.
21 P. Björk, K. P. R. Nilsson, L. Lenner, B. Kågedal, B. Persson, O. Inganäs and J. Jonasson, *Mol. Cell. Probes*, 2007, **21**, 329–337.
22 Y. Wang, L. Feng and S. Wang, *Adv. Funct. Mater.*, 2019, **29**, 1806818.
23 T. V. Richter, C. Bühler and S. Ludwigs, *J. Am. Chem. Soc.*, 2012, **134**, 43–46.
24 C. A. Traina, B. R. Nd and G. C. Bazan, *J. Am. Chem. Soc.*, 2011, **133**, 12600–12607.
25 J. Wang, F. Lv, L. Liu, Y. Ma and S. Wang, *Coord. Chem. Rev.*, 2018, **354**, 135–154.
26 A. Nanid, S. Das, D. P. Chatterjee and R. Ghosh, *RSC Adv.*, 2015, **5**, 20160–20177.

27 S. Das, P. Routh, R. Ghosh, D. P. Chatterjee and A. K. Nandi, *Polym. Int.*, 2017, **66**, 623–639.
28 S. Li, T. Chen, Y. Wang, L. Liu, F. Lv, Z. Li, Y. Huang, K. S. Schanze and S. Wang, *Angew. Chem., Int. Ed. Engl.*, 2017, **56**, 13455–13458.
29 C. Zhu, L. Liu, Q. Yang, F. Lv and W. Shu, *Chem. Rev.*, 2012, **112**, 4687–4735.
30 I. B. Kim and S. A. J. Garcia, *Bioconjugate Chem.*, 2007, **18**, 815–820.
31 K. Y. Pu, K. Li and B. Liu, *Adv. Funct. Mater.*, 2010, **20**, 2770–2777.
32 R. Hu, S. Li, H. Lu, L. Liu, F. Lv and S. Wang, *Mater. Chem. Front.*, 2017, **1**, 1768–1772.
33 M. Zhang, P. Wu, W. T. Dou, H. H. Han and Y. Jiang, *Chem. Commun.*, 2017, **53**, 5625–5628.
34 L. Liu, Q. Zhang, J. Wang, L. Zhao, L. Liu and Y. Lu, *Talanta*, 2019, **198**, 128–136.
35 F. Wang, Z. Liu, B. Wang, L. Feng, L. Liu, F. Lv, Y. Wang and S. Wang, *Angew. Chem., Int. Ed. Engl.*, 2014, **53**, 424–428.
36 F. Wang, M. Li, B. Wang, J. Zhang, Y. Cheng, L. Liu, F. Lv and S. Wang, *Sci. Rep.*, 2015, **5**, 7617.